2009

Oxidative dissolution potential of biogenic and abiogenic TcO2 in subsurface sediments

James K. Fredrickson
Pacific Northwest National Laboratory, jim.fredrickson@pnl.gov

John M. Zachara
Pacific Northwest National Laboratory, john.zachara@pnl.gov

Andrew Plymale
Pacific Northwest National Laboratory, andrew.plymale@pnl.gov

Steve M. Heald
Argonne National Laboratory

James Mckinley
Pacific Northwest National Laboratory, james.mckinley@pnl.gov

See next page for additional authors

Available online at www.sciencedirect.com
ScienceDirect
Geochimica et Cosmochimica Acta 73 (2009) 2299–2313
Geochimica et Cosmochimica Acta
www.elsevier.com/locate/gca

Oxidative dissolution potential of biogenic and abiogenic TcO_2 in subsurface sediments

James K. Fredrickson [a,*], John M. Zachara [a], Andrew E. Plymale [a], Steve M. Heald [b], James P. McKinley [a], David W. Kennedy [a], Chongxuan Liu [a], Ponnusamy Nachimuthu [a]

[a] *Pacific Northwest National Laboratory, P.O. Box 999, MSIN P7-50, Richland, WA 99352, USA*
[b] *Argonne National Laboratory, Argonne, IL 60439, USA*

Received 5 August 2008; accepted in revised form 27 January 2009; available online 8 February 2009

Abstract

Technetium-99 (Tc) is an important fission product contaminant associated with sites of nuclear fuels reprocessing and geologic nuclear waste disposal. Tc is highly mobile in its most oxidized state [$Tc(VII)O_4^-$] and less mobile in the reduced form [$Tc(IV)O_2{\cdot}nH_2O$]. Here we investigate the potential for oxidation of Tc(IV) that was heterogeneously reduced by reaction with biogenic Fe(II) in two sediments differing in mineralogy and aggregation state; unconsolidated Pliocene-age fluvial sediment from the upper Ringold (RG) Formation at the Hanford Site and a clay-rich saprolite from the Field Research Center (FRC) background site on the Oak Ridge Site. Both sediments contained Fe(III) and Mn(III/IV) as redox active phases, but FRC also contained mass-dominant Fe–phyllosilicates of different types. *Shewanella putrefaciens* CN32 reduced Mn(III/IV) oxides and generated Fe(II) that was reactive with Tc(VII) in heat-killed, bioreduced sediment. After bioreduction and heat-killing, biogenic Fe(II) in the FRC exceeded that in RG by a factor of two. More rapid reduction rates were observed in the RG that had lower biogenic Fe(II), and less particle aggregation. EXAFS measurements indicated that the primary reduction product was a TcO_2-like phase in both sediments. The biogenic redox product Tc(IV) oxidized rapidly and completely in RG when contacted with air. Oxidation, in contrast, was slow and incomplete in the FRC, in spite of similar molecular scale speciation of Tc compared to RG. X-ray microprobe, electron microprobe, X-ray absorption spectroscopy, and micro X-ray diffraction were applied to the whole sediment and isolated Tc-containing particles. These analyses revealed that non-oxidizable Tc(IV) in the FRC existed as complexes with octahedral Fe(III) within intra-grain domains of 50–100 μm-sized, Fe-containing micas presumptively identified as celadonite. The markedly slower oxidation rates in FRC as compared to RG were attributed to mass-transfer-limited migration of O_2 into intra-aggregate and intraparticle domains where Tc(IV) existed; and the formation of unique, oxidation-resistant, intragrain Tc(IV)–Fe(III) molecular species.

1. INTRODUCTION

^{99}Tc is a long-lived ($t^{1/2} = 2.13 \times 10^5$ years) fission product generated as a result of nuclear production and reprocessing. At the US Department of Energy's Hanford Site and other DOE sites across the US (Riley and Zachara, 1992) and at nuclear facilities world-wide, ^{99}Tc contamination is of particular concern because it can migrate rapidly with vadose zone water and groundwater as pertechnetate [$Tc(VII)O_4^-$] (Evans et al., 2007; Zachara et al., 2007a). At Hanford, over 500 Ci of $Tc(VII)O_4^-$ released to the vadose zone in past site operations are forecast to be mobile in predominantly oxidizing groundwaters with eventual discharge to the Columbia River (Khaleel et al., 2007), making it one of the site's major risk-driving contaminants. The subsurface inventory and behavior of ^{99}Tc at Hanford,

* Corresponding author. Fax: +1 509 376 7063.
E-mail address: jim.fredrickson@pnl.gov (J.K. Fredrickson).

0016-7037/$ - see front matter © 2009 Elsevier Ltd. All rights reserved.
doi:10.1016/j.gca.2009.01.027

and associated water quality and health risk issues, have been well described in a recent journal issue devoted entirely to the Hanford Site (Gee et al., 2007).

Under anoxic conditions, some microorganisms (Lloyd and Macaskie, 1996; Lloyd et al., 1997; Lloyd et al., 1999; Wildung et al., 2000; Marshall et al., 2008) can couple the oxidation of H_2 or organic compounds to the reduction of $Tc(VII)O_4^-{}_{(aq)}$ to an oxide precipitate [$Tc(IV)O_2{\cdot}nH_2O$ with solubility $\sim 10^{-8}$ mol/L] and, subject to factors such as bicarbonate concentration and pH, soluble Tc(IV) carbonate complexes (Wildung et al., 2000). Depending on the organism and incubation conditions, $Tc(IV)O_2{\cdot}nH_2O$ nanoparticles are the primary product, typically formed in association with the cell envelope and periplasm of gram-negative bacteria (Lloyd et al., 2000; Wildung et al., 2000; Marshall et al., 2009).

In soils and sediments, the complexity of biogeochemical properties and reactions makes it difficult to predict whether direct enzymatic or indirect [i.e., by Fe(II)] reduction reactions of $Tc(VII)O_4^-{}_{(aq)}$ will predominate (Wildung et al., 2004; Burke et al., 2005). Fe(III) and Mn(III/IV) oxides in particular can impart substantial control on reactive contaminant behavior in soils and sediments, in that they can constitute a substantial redox buffering capacity (Heron et al., 1995). As these environments become progressively reducing, increasing concentrations of Fe(II) are generated as a result of microbial metabolism. Depending on the form of Fe(II), it can serve as a facile reductant of TcO_4^-. For example, nanocrystalline magnetite, as a product of microbially reduced ferrihydrite, was shown to effectively reduce Tc(VII) to an insoluble form (Lloyd et al., 2000), and sediment-associated Fe(II) was implicated as the principal reductant of TcO_4^- in anoxic US Atlantic Coastal Plain sediments (Wildung et al., 2004). In previous investigations, we reported the reduction of TcO_4^- by biogenic Fe(II) associated with subsurface sediments from US DOE sites (Hanford and Oak Ridge) and other locations (Fredrickson et al., 2004). Rates of TcO_4^- reduction generally increased with increasing concentrations of 0.5 N HCl-extractable Fe(II), but marked differences in rates between sediments with different mineralogy implied that sorbed Fe(II) associated with residual Fe(III) oxides was more reactive than that associated with layer silicates. This hypothesis was verified by Peretyazhko et al. (2008a), who found that heterogeneous reduction rates of Tc(VII) by Fe(II) adsorbed on hematite and goethite were orders of magnitude more rapid than for structural Fe(II) in phyllosilicates.

It is clear from these previous reports that reduction of TcO_4^- to poorly soluble $Tc(IV)O_2{\cdot}nH_2O$, either by direct or indirect microbial-mediated reduction reactions, has the potential to impede the migration of ^{99}Tc in the subsurface. In one of the first demonstrations of in situ reduction of Tc(VII) Istok et al. (2004), stimulated microbial activity, via the addition of ethanol, glucose or acetate, in contaminated subsurface sediments at DOE's Oak Ridge site and observed decreasing concentrations of Tc(VII) in groundwater, indicative of reductive immobilization. What remains uncertain is the fate of ^{99}Tc in microbially reduced sediments if and when aerobic waters infiltrate into reduced sediments.

The purpose of this research was to investigate the potential for O_2-promoted oxidation of biogenic Tc(IV)$O_2{\cdot}nH_2O$ nanoparticles and Tc(IV) resulting from abiotic reactions with sediment-associated Fe(II). The rates of oxidation of the various biogenic and abiogenic forms of Tc(IV) were investigated, as was the form and distribution of residual, sorbed Tc remaining after an extended period of air oxidation. This information contributes to the understanding of the fate of $^{99}Tc(VII)$ in subsurface sediments subject to fluctuating redox conditions or where remedial actions taken to stimulate reduction are followed by a period of re-equilibration with aerobic groundwater.

2. EXPERIMENTAL PROCEDURES

2.1. Soils and sediments

Unconsolidated Pliocene-age fluvial sediment from the upper Ringold (RG) Formation, referred to as Ringold 6–6/6–7, was obtained near the Hanford Site from White Bluffs outcrops approximately 60 m above the Columbia River. The Fe(III) and Mn(III/IV) oxide mineralogy of this sand-textured, mica-containing sediment was reported by Zachara et al. (1998) and Fredrickson et al. (2004). A clay-rich saprolite was obtained from the Field Research Center (FRC) background site located in the West Bear Creek Valley on the Oak Ridge Site in eastern Tennessee. This material is referred to as FRC saprolite. Nearby TcO_4^- and UO_2^{2+} plumes exist in these same sediment types (Istok et al., 2004; RPP, 2005; Zachara et al., 2007c). The aggregated, weakly cemented subsurface materials were air-dried, ground, and passed through a 2 mm sieve prior to use. The mineralogic and chemical characterization of the FRC has been described elsewhere (Fredrickson et al., 2004; Kukkadapu et al., 2006).

2.2. Bacteria and media

Shewanella putrefaciens strain CN32 was provided courtesy of Dr. David Boone (Subsurface Microbial Culture Collection, Portland State University, Portland, OR). Strain CN32 was isolated from a subsurface core sample (250 m beneath the surface) from the Morrison Formation in northwestern New Mexico (Fredrickson et al., 1998) and was used previously for investigations of the biogenic Fe(II)-facilitated reduction of Tc(VII) (Fredrickson et al. 2004). For these experiments, CN32 was routinely cultured aerobically in tryptic soy broth (TSB), 30 g L^{-1} (Difco Laboratories, Detroit, MI), and stock cultures were maintained by freezing in 40% glycerol at −80 °C. For batch experiments, CN32 cells were harvested from TSB cultures at mid to late log phase by centrifugation, washed twice with 30 mM pH 7 PIPES buffer and once with 30 mM pH 7 bicarbonate buffer to remove residual medium. The cells were then suspended in bicarbonate buffer and purged with O_2-free N_2:CO_2 (80:20).

2.3. Technetium reduction–oxidation experiments

Bioreduced sediments (in triplicate) were generated by incubating 0.5 g (RG, 50 g/L) or 1 g (FRC, 100 g/L) sediment in 10 ml of 30 mM pH 7 bicarbonate or 30 mM pH

7 PIPES buffer with $7–9 \times 10^7$ cells/ml *S. putrefaciens* CN32 and 10 mM sodium lactate as electron donor, with a N_2:CO_2 (80:20, bicarbonate) or N_2 (100%, PIPES) headspace, both O_2-scrubbed, at 30 °C with shaking at 25 rpm.

At select time points, bioreduced sediments were pasteurized by heating at 80 °C for 1 h and then frozen at −20 °C until used. Viable cells of CN32 could not be detected by growth on TSB agar plates following pasteurization. Abiotic Tc reduction experiments were initiated by adding 0.5 ml of a stock of anaerobic ammonium pertechnetate, $NH_4{}^{99}TcO_4$, at a concentration needed to give the final desired concentration. The stock solutions were added to the 10-ml sediment slurries using a 22-ga. needle and 1-cc syringe. After abiotic reduction was complete, oxidation in air was initiated by passive venting of the glass pressure tube by inserting an 18-ga. needle through the butyl rubber stopper fitted with a 0.2 μm syringe filter (Gelman) to prevent the entry of airborne microorganisms, with the filter outlet covered with Parafilm® to retard evaporation. Oxygen entry into the anoxic tube was, consequently, diffusion controlled. Samples were incubated on their sides on a gyratory shaker at 25 rpm. The experiments measuring oxidation of biogenic $TcO_2{\cdot}nH_2O$, prepared as previously described (Fredrickson et al., 2004), were conducted in air-saturated 30 mM bicarbonate in sealed pressure tubes with an air headspace or in anoxic bicarbonate buffer with unreduced sediment (1 g) in sealed tubes and a N_2:CO_2 (80:20) headspace.

The concentrations of Fe and Mn in aqueous filtrates (0.2 μm) and 0.5 N HCl extracts (1 h, agitated at 25 rpm) were measured by ICP-AES and Fe(II) was measured by the ferrozine assay. Soluble Tc was measured filtering subsamples through a 0.2 μm syringe filter (Gelman) and assaying by liquid scintillation counting. The minimum quantifiable $[Tc]_{aq}$ concentration in the absence of preconcentration was 0.04 μM, corresponding to a background of 20 dpm. We note that the solubility of $TcO_2{\cdot}nH_2O$ may increase by a maximum of 0.4 log units from $10^{-8.15}$ to $10^{-7.75}$ M in the bicarbonate-buffered sediment suspension through formation of Tc(IV)–carbonate complexes (Liu et al., 2007). Our liquid scintillation counting procedure for Tc aqueous phase quantification was not of sufficient precision or accuracy at these concentrations to distinguish any difference in Tc(IV) solubility in the two buffers used.

2.4. Mössbauer spectroscopy

Samples were prepared for analysis by filtration (0.22 μm), washing with acetone, and drying in an anaerobic glovebox with <0.5 ppm O_2. Random orientation absorbers were prepared by mixing 100–200 mg of dried sample with petroleum jelly in a 0.5-in. thick and 0.5-in. ID Cu holder sealed at one end with clear scotch tape. The sample space was filled with petroleum jelly and the ends sealed with the tape. The bioreduced samples were handled under an anaerobic atmosphere. Spectra were collected at room temperature (RT) using ~50 mCi (1.85 GBq) (initial strength) ^{57}Co/Rh single-line thin sources. The velocity transducer (MVT-1000; WissEL) was operated in the constant-acceleration mode. Data were acquired on 1024 channels and then folded to 512 channels to give a flat background and a zero-velocity position corresponding to the center shift (CSδ) of a metallic-Fe foil at room temperature. Calibration spectra were obtained with a 20-μm thick α-Fe foil (Amersham, England) placed in exactly the same position as the samples to minimize any error due to changes in geometry. The transmitted radiation was recorded with an Ar–Kr proportional counter. The unfolded spectra obtained were folded and evaluated with the Recoil program (University of Ottawa, Canada) using a Voigt-based hyperfine parameter distribution method.

2.5. XANES, EXAFS, X-ray microprobe (XRM), and micro X-ray diffraction analyses

Synchrotron based measurements were performed at Sector 20 of the Advanced Photon Source (APS) at Argonne National Laboratory including: (i) bulk Tc-K edge XANES and EXAFS on bioreduced/Tc(VII)-reacted FRC and Ringold sediments before oxidation, and the Tc(VII)-reacted FRC sediment after oxidation on bending magnet beamline 20-BM, (ii) micro-Tc XANES and XRM elemental mapping of Tc, Fe, and Rb (based on K_α-fluorescence) of 60 μm thin sections of the oxidized FRC sediment (mounted on high purity fused silica slides) on insertion device beamline 20-ID, and (iii) XRM elemental mapping, micro-Tc XANES, and micro-Tc EXAFS of 27, mm-sized particles isolated from the oxidized, Tc(VII)-reacted FRC sediment on beamline 20-ID [including those suspected and not suspected to contain oxidation-resistant Tc(IV)]. These measurements used anaerobic sample mounting procedures; incident X-ray fluxes, beam-line procedures, and calibration methods; and a variety of Tc(IV) standards described in Fredrickson et al. (2004), Zachara et al. (2007b), Peretyazhko et al. (2008a,b).

Four Tc-containing particles of approximate 50–100 μm size that were isolated from oxidized FRC sediment and that yielded good micro-Tc EXAFS spectra as described above were individually mounted on a flat metallic planchette and analyzed in reflection mode on a Rigaku (The Woodlands, TX) D/MAX-RAPID II X-ray microdiffraction system. Copper Kα X-rays were generated using a 1200 W rotating anode source and collimated to 100 μm on the sample surface, with diffraction pattern collection onto a 2-D detector. Data reduction and phase identification was by Jade software (Molecular Dynamics, Livermore, CA) against the ICDD PDF-2 X-ray diffraction database.

3. RESULTS

3.1. Oxidation of biogenic $Tc(IV)O_2{\cdot}nH_2O$

Previously, we reported the oxidation of nanoparticulate, biogenic $Tc(IV)O_2{\cdot}nH_2O$ in anoxic but unreduced FRC saprolite, with 70% of an initial 20 μM suspension being oxidized to TcO_4^- over the course of a 41 d equilibration period (Fredrickson et al., 2004). This oxidation was apparently promoted by solid-phase electron transfer between $Tc(IV)O_2{\cdot}nH_2O$ and Mn(III/IV) oxide particles in

the sediment. In the current study, we extended these experiments to include equilibrations of biogenic Tc(IV)$O_2{\cdot}nH_2O$ with: (i) anoxic, unreduced Ringold sediment, and (ii) air-saturated suspensions. The oxidation of Tc(IV)$O_2{\cdot}nH_2O$ in air-saturated buffer was relatively rapid (Fredrickson et al., 2004), with >75% of the initial 20 μM suspension being oxidized to $TcO_4^-{}_{(aq)}$ within 6 d; the remainder was oxidized more slowly over the remaining 33 d of the experiment (Fig. 1a), suggesting the presence of a less reactive fraction. In anoxic, unreduced Ringold suspension, the oxidation was slower than in air-saturated water, but more rapid than previously reported for anoxic, unreduced FRC saprolite. This difference was likely due to the relative abundance and exposure of Mn oxides in these two samples, with 171 and 33 μmol/g sediment of hydroxylamine–HCl extractable Mn (readily reducible hydrous Mn oxide; Chao, 1972; Gambrell, 1996) in the Ringold and FRC materials, respectively.

In a separate experiment, 1.0 mM of biogenic Tc(IV)$O_2{\cdot}nH_2O$ was added to an unreduced anoxic FRC saprolite suspension to investigate its potential for oxidizing Tc(IV). Assuming that the hydroxylamine–HCl extractable Mn in the FRC sediment (33.2 μmol/g; Fredrickson et al., 2004) was all Mn(IV), there would have been approximately a twofold stoichiometric excess of Mn(IV) for oxidizing Tc(IV) to Tc(VII). Over an extended 312 d equilibration period, slightly less than 50% of the biogenic Tc(IV)$O_2{\cdot}nH_2O$ was oxidized to soluble Tc(VII), indicating that factors other than total electron equivalents from Mn(III/IV) were controlling Tc(IV) oxidation (Fig. 1b). However, these sediments have been previously shown to be highly aggregated (Fredrickson et al., 2004; Kukkadapu et al., 2006), and it is possible that hydroxylamine–HCl extractable Mn(III/IV) oxides existed in intra-aggregate domains that prevented contact with non-diffusible Tc(IV)$O_2{\cdot}nH_2O$.

3.2. TcO_4^- reduction capacity of bioreduced FRC sediment

Given the previous report of near-instantaneous reduction of 20 μM TcO_4^- in 36 d bioreduced FRC sediment (Fredrickson et al., 2004), the capacity for Tc(VII) reduction was further investigated in bioreduced FRC (60 d) and Ringold (120 d) materials via consecutive additions, within a 17 d period, of increasing concentrations (50, 500, and 1250 μM) of ammonium pertechnetate (Fig. 2). The initial data point for each concentration in series represents the $Tc(VII)_{aq}$ concentration remaining after 2–4 min of contact with the pasteurized, bioreduced sediment. The reduction of the initial 50 μM and 500 μM TcO_4^- in the Ringold sediment was near instantaneous (Fig. 2, inset) whereas reduction of the subsequent high concentration spike (1250 μM) occurred rapidly over an approximate 11 d period. The Tc(VII) reduction rate was slower in the FRC for all spike concentrations, but all Tc(VII) was eventually reduced. In the Ringold sediment following the addition of a total of 1.8 mM TcO_4^-, the concentration of

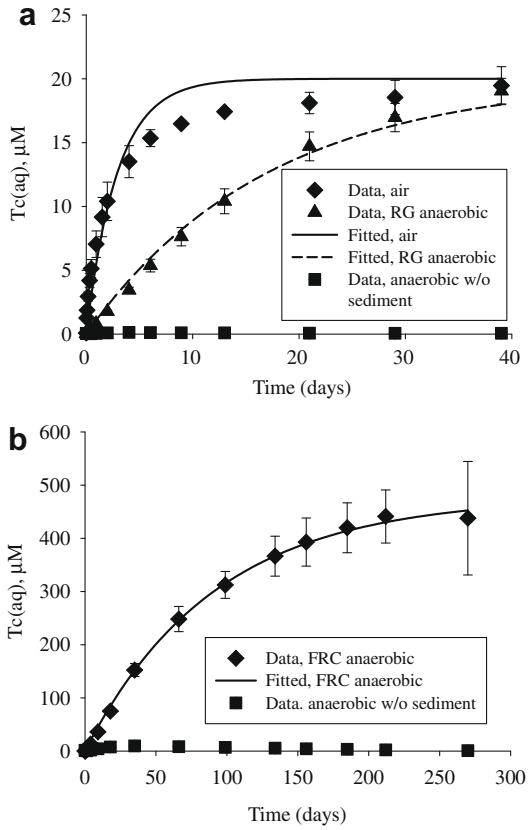

Fig. 1. (a) Oxidative solubilization of biogenic $TcO_2{\cdot}H_2O_{(s)}$ (20 μM) in air or anaerobically (N_2:CO_2, 80:20) with or without RG sediment in 30 mM $NaHCO_3$, pH 7 buffer, and (b) oxidative solubilization of biogenic $TcO_2{\cdot}H_2O_{(s)}$ (1.0 mM) in anaerobic (O_2-scrubbed N_2) FRC sediment suspension in 30 mM, pH 7, PIPES. Solid and dashed lines represent pseudo first-order kinetic model fitting of the data with results in Table 1.

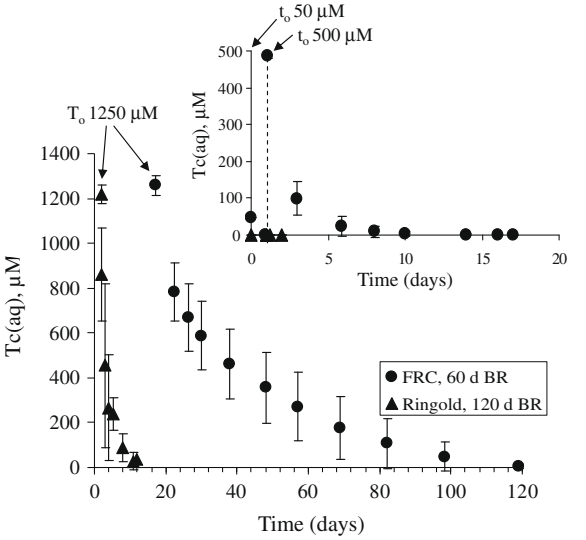

Fig. 2. Reduction capacity of FRC and Ringold sediments bioreduced in 30 mM pH 7 PIPES buffer for 60 and 120 d, respectively, then exposed to consecutive spikes of 50, 500 (inset), and 1250 μM TcO_4^-. *Note*: Initial 0.5 N HCl Fe(II) was 11.99 ± 0.86 mM for FRC and 5.39 ± 0.79 mM for RG. Electron equivalents required for full reduction of all added Tc(VII) was 5.1 mM. t_0 is time of spiking.

soluble Tc was <40 μM after 12 d whereas in the FRC saprolite an equilibration period of >98 d was required to bring the $TcO_4^-{}_{(aq)}$ concentration to below 40 μM. The pH over the course of the reduction phase of the experiment ranged from 7.4 to 7.9 for both sediments and the 0.5 N HCl-extractable Fe(II) concentrations were 12.0 ± 0.9 mM (or 0.12 mmol/g) and 5.4 ± 0.8 mM (or 0.11 mmol/g) for the FRC and Ringold materials, respectively. For the Ringold sediment at least 95% of the biogenic Fe(II) pool had thermodynamic power to reduce Tc(VII), and was fast to react. Consequently, both sediments have an extensive capacity for Fe(II)-facilitated TcO_4^- reduction given that typical Tc(VII) environmental concentrations are generally less than 10^{-5} mol/L, and often much less. These results are also consistent with previous findings (Fredrickson et al., 2004) in that the solid-phase 0.5 N HCl extractable Fe(II) in the FRC saprolite was much less reactive than Ringold Fe(II).

3.3. Oxidation of Tc(IV) reduced by biogenic Fe(II)

TcO_4^-, added as 20 μM ammonium pertechnetate, was reacted with pasteurized, bioreduced FRC and Ringold materials in 30 mM $NaHCO_3$ (pH ~ 7, and N_2:CO_2 of 80:20), to allow for quantitative reduction to Tc(IV). After reduction was confirmed by a decrease in the concentration of aqueous Tc to below detection (~0.04 μM), pressure tubes were vented to the atmosphere and the oxidative solubilization of Tc measured with time. In the pasteurized Ringold sediment, 65% of the Tc(IV) was released to the aqueous phase within 14 d, followed by a slower oxidation period, where all of the initial 20 μM Tc was solubilized within 112 d (Fig. 3a). In contrast, the rate of oxidative solubilization of Tc(IV) from bioreduced FRC saprolite was considerably slower, with <35% of the initial Tc(IV) released after 97 d of air exposure.

Significant differences were therefore noted in the oxidation of abiotically, heterogeneously reduced/precipitated Tc(IV) in the two sediments. We reasoned that this effect may have resulted, in part, from differences in the concentration of biogenic Fe(II) in the two sediments that influenced their redox buffering capacities. The rate of oxidation of biogenic Fe(II) was investigated in a separate experiment in the absence of Tc. In this experiment, 0.5 N HCl-extractable Fe(II) declined from 10.7 mM to 3.2 mM after 38 d in the FRC saprolite, and then to 1.3 mM after 270 d. Biogenic Fe(II) declined from 4.7 mM in the Ringold sediment to less than 240 μM in 34 d (Fig. 3b).

In a separate experiment, ~1 mM TcO_4^- was added to bioreduced FRC and Ringold materials, equilibrated until the concentration of soluble Tc was below 1 μM (0.28 ± 0.19 and 0.26 ± 0.06 μM for FRC and RG, respectively), and then exposed to air to probe the rate and extent of oxidative solubilization of Tc(IV). Consistent with the results from experiments where increasing concentrations of TcO_4^- were consecutively added to sediments, the rate of Tc reduction was much more rapid in the 120 d bioreduced Ringold sediment than the 60 d bioreduced FRC sediment, with the former being quantitatively reduced in 2 days and the later requiring approximately 40 d

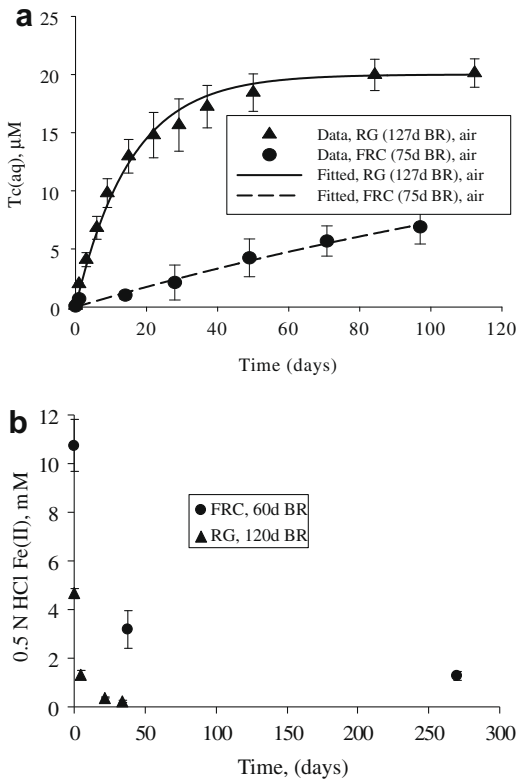

Fig. 3. (a) Oxidative solubilization of biogenic Fe(II)-reduced TcO_4^- (20 μM) in 30 mM $NaHCO_3$ pH 7 buffer (N_2:CO_2, 80:20 headspace) in FRC, bioreduced for 75 d, and RG, bioreduced for 127 d, sediment continuously exposed to air; solid and dashed lines represent pseudo first-order kinetic model fitting of the data with results in Table 1, and (b) oxidation of 0.5 N HCl-extractable Fe(II) in 30 mM, pH 7, PIPES buffer in FRC, bioreduced for 60 d, and RG, bioreduced for 120 d, sediment continuously exposed to air.

(Fig. 4a). During the oxidation phase, Tc(IV) associated with the Ringold sediment was released more rapidly and extensively than in the FRC saprolite (Fig. 4b) with essentially all of the Tc originally added being released within 40 d. In contrast, approximately 25% of the Tc remained associated with the FRC saprolite even after equilibration for 227 d.

Room temperature Mössbauer spectroscopy measurements on the FRC sediment provided additional insights on Fe valence dynamics during bioreduction and oxidation by both Tc(VII) and O_2 (Fig. 5). The unreduced FRC sediment contained two Mössbauer doublets (Fig. 5a) resulting from Fe(III) (90% Fe-total; in phyllosilicates, small-particle or Al-goethite, and minor peaks 3 and 4 of hematite sextet) and Fe(II) [10% Fe-total; residing in both large and small sized phyllosilicates, (Kukkadapu et al., 2006)]. Bioreduction increased the Fe(II) doublet (to 28%) relative to Fe(III) (72%), Fig. 5b, through both Fe(III) oxide and phyllosilicate reduction (Kukkadapu et al., 2006). Reaction with $Tc(VII)O_4^-$ proportionally decreased Fe(II) (to 20%, Fig. 5c), while air contact returned the Fe valence distribution back to the original state (Fig. 5d) (Komlos et al., 2007). It was not resolved whether the residual Fe(II) noted

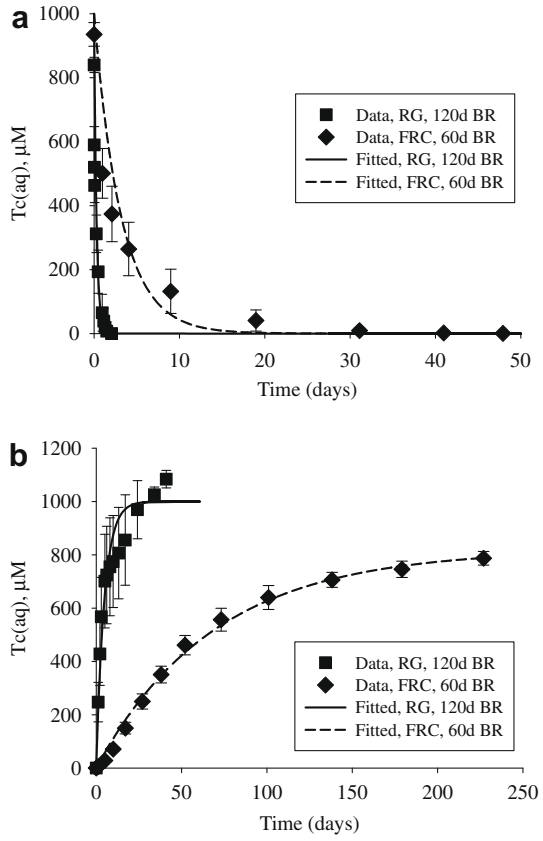

Fig. 4. (a) Reduction of ~1 mM TcO_4^- in pasteurized FRC and RG sediment in 30 mM, pH 7 PIPES buffer, and (b) Oxidative solubilization of biogenic Fe(II)-reduced TcO_4^- (~1 mM) in FRC, bioreduced for 60 d, and RG, bioreduced for 120d, sediment continuously exposed to air. Solid and dashed lines represent pseudo first-order kinetic model fitting of the data with results in Table 1.

in Fig. 3b (e.g., 1.3 mM) was the same mineral component as that observed in Fig. 5d.

3.4. Kinetic analysis

The reduction and oxidation experiments in Figs. 1a and b, 3a, 4a and b were described with a pseudo first-order kinetic model (Zachara et al., 2007b; Peretyazhko et al., 2008a) that fit the data well. The intent of this modeling was to quantitatively compare the rates of Tc oxidation (primarily) and reduction at different Tc concentrations and under different conditions. Four primary conclusions were evident through comparisons of the resulting first-order rate constants (Table 1). Tc(VII) reduction rates in both sediments were over an order of magnitude more rapid than Tc(IV) oxidation. Second, Tc reduction and oxidation rates in the FRC sediment were approximately 10-fold slower than in the Ringold sediment. Moreover, two of the Tc(IV) oxidation experiments with the FRC required a two-parameter fit where only a fraction of the Tc(IV) was considered oxidizable. Third, Tc(IV) oxidation rates in both sediments increased by a factor of 3 with a 50-fold increase in Tc(IV) concentration. Fourth, the Tc(IV) oxidation rate in the Ringold sediment at the highest concentration (1000 μM) was equivalent to that of biogenic Tc(IV)·nH_2O in air-saturated buffer suspension.

3.5. Molecular speciation and mineral association of recalcitrant Tc(IV)

Bulk K-edge Tc-XANES analyses of the Tc(VII)-spiked FRC (after 50 d) and the RG (after 3 d) revealed that all sorbed Tc was in the tetravalent state [Tc(IV), see Electronic Annex Fig. EA-1-1]. The transforms of bulk Tc-EXAFS of the two sediments were virtually identical to one another (Fig. 6), and to that of heterogeneously precipitated Tc on a dithionite–citrate–bicarbonate (DCB)-reduced phyllosilicate isolate from the FRC sediment (Peretyazhko et al., 2008a) that contained smectite, vermiculite, illite, and micas (Kukkadapu et al., 2006) [see Electronic Annex Fig. EA-1-2 for k^2 weighted $\chi(k)$ data]. The spectra bore similarities to that of abiotic standard Tc(IV) O_2·nH_2O (Fig. 6), but were different from heterogeneously reduced/precipitated Tc on Fe(III) oxides (Peretyazhko et al., 2008a). The Tc-EXAFS spectra for the two sediments were modeled with the Tc-chain model approach described by Peretyazhko et al. (2008a) and originally by Lukens et al. (2002). The fitting details are provided in Electronic Annex Table EA-1-1 and an example of such a fit in Fig. EA-1-3. This approach interprets the Tc-EXAFS spectra of both sediments to result from sorbed polymeric chains of TcO_2 octahedra with average chain length above that of a dimer, but below that of homogeneous, abiotic Tc(IV)O_2·nH_2O precipitate. In these samples the average chain length was approximately 3 (trimers). The molecular speciation of heterogeneous Tc(IV) in both sediments was the same within error. The unshifted FT-peak at 1.5 Å results from first shell octahedral O, the peak at 2.3 Å from second shell Tc–Tc interactions and Tc–metal interactions with the substrate, and the peaks at 2.7–3.2 Å from multiple scattering within the Tc–O octahedra and axial O in the neighboring octahedra. The intensity of the second peak is determined by interference between the Tc–Tc signals and the Tc–metal bond in the substrate. These tend to cancel each other when the amount of Tc–Tc bonding (small average chain length) is reduced.

Bulk XANES analyses of water-extracted FRC sediment from Fig. 4b after 270 d of air oxidation revealed that all residual, sorbed Tc in the sediment existed as Tc(IV) (data not shown). Thin sections of the oxidized sediment were analyzed by X-ray microprobe (XRM). Tc was clearly visible in thin section as isolated "hot-spots" of 25–100 μm size (see Electronic Annex Figs. EA-1-4 and EA-1-5), invariably in association with discrete mineral grains or aggregates that contained Fe and Rb. Rubidium (Rb^+) is a common trace substituent for K^+ in micas that is accessible to XRM through its Kα fluorescence at 13,395 eV. The comparable Kα fluorescence for K^+ at 3314 eV is blocked by the kapton windows used for containment of the radioactive sample. Consequently, Rb was used as a surrogate for K^+, with the reasonable assumption that Rb distribution and

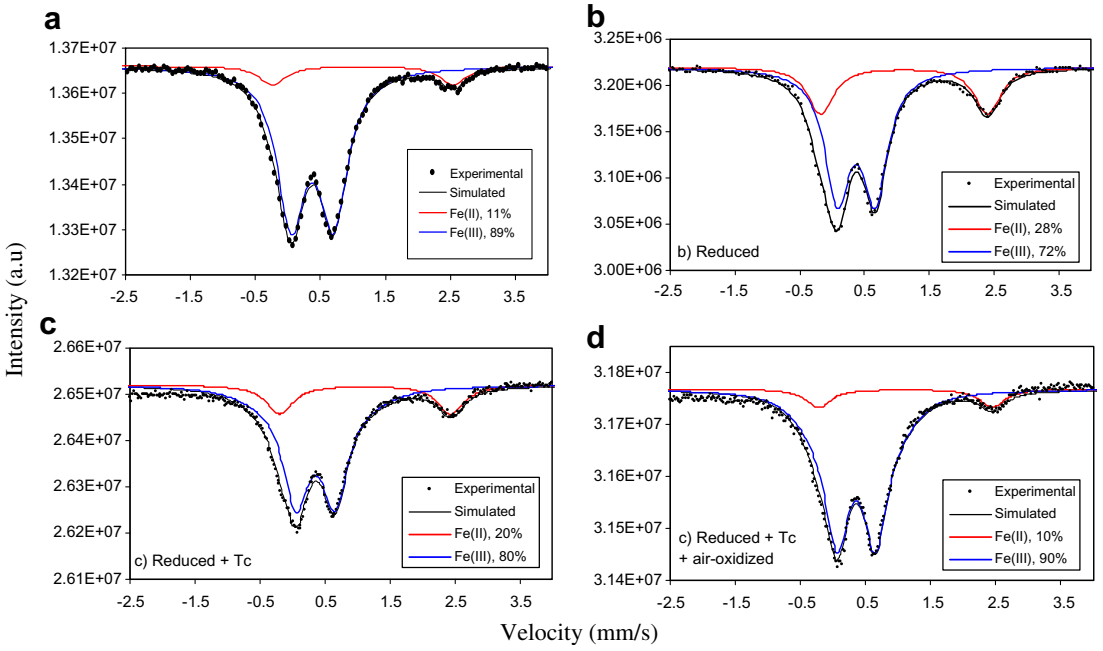

Fig. 5. ^{57}Fe Mössbauer spectroscopy of FRC sediment: (a) unreduced, (b) bioreduced in 30 mM pH 7 PIPES buffer for 60 d, (c) bioreduced for 60 d and then exposed to 1 mM TcO_4^-, and (d) bioreduced, exposed to 1 mM TcO_4^-, and subsequently exposed to air for 270 d.

Table 1
Pseudo first-order rate constants for the Tc reduction/oxidation reactions.

Initial		First-order rate constant (d^{-1})
Biogenic Tc(IV) oxidation (Fig. 1)		
Air	Tc(IV) = 20 μM	3.42×10^{-1}
RG	Tc(IV) = 20 μM	5.87×10^{-2}
FRC	Tc(IV) = 1000 μM[a]	1.09×10^{-2}
Tc(IV) oxidation in bioreduced sediment (Fig. 3a)		
RG	Tc(IV) = 20 μM	6.45×10^{-2}
FRC	Tc(IV) = 20 μM	4.51×10^{-3}
Tc(VII) reduction by bioreduced sediment (Fig. 4a)		
RG	Tc(VII) = 1000 μM	3.50
FRC	Tc(VII) = 1000 μM	3.15×10^{-1}
Tc(IV) oxidation in bioreduced sediment (Fig. 4b)		
RG	Tc(IV) = 1000 μM	2.09×10^{-1}
FRC	Tc(IV) = 1000 μM[b]	1.45×10^{-2}

[a] 477 μM was oxidizable.
[b] 819 μM was oxidizable.

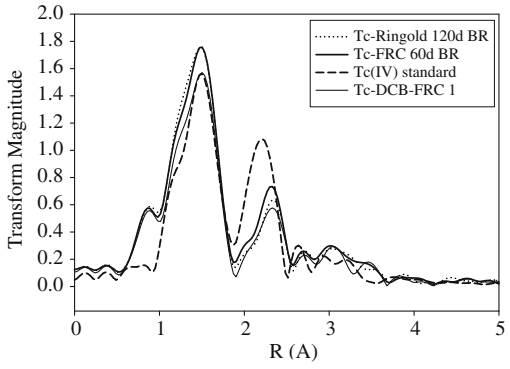

Fig. 6. Fourier transform (FT) EXAFS spectra for sorbed Tc on bioreduced FRC and Ringold sediments as compared to abiotic standard $TcO_2 \cdot nH_2O$, and heterogeneously reduced Tc on a DCB-reduced, phyllosilicate isolate from the FRC 1 sediment [from Peretyazhko et al. (2008b)].

spatial location mimicked that of K. Micro-XANES analyses of these "hot-spots" displayed that all were comprised of Tc(IV) (Fig. 7). Further characterization of the Tc-containing particles in thin section proved challenging, because typically only a small portion of each particle was exposed at the section surface. The Tc-containing phase was hypothesized to be Fe-containing mica, because of its size, Rb signal indicating high K content, and previous identification of mica in the FRC sediment (Kukkadapu et al., 2006).

Individual mineral grains (18) with size and morphology consistent with that of mica were hand-picked from the Tc-containing, air-oxidized sediment using a binocular, optical microscope. These were mounted, grouped to the left side of a thin plastic disc, within kapton-faced wells, which were numbered and labeled as "probable." Another set of mineral grains (9) of similar size were randomly picked from the sediment, mounted comparably and grouped to the right side of the disc, and labeled as "other". Thirteen of the "probable" wells were surveyed for Tc (along with selected, co-associated elements), using XMP. Particles were located within 11 of the 13 wells, of which 10 were positive for Tc (and Fe). For the "other" particles, 3 of 5 surveyed wells also showed the presence of Tc (and Fe).

While all Tc-containing particles contained Fe and Rb in association, three particle types were qualitatively differentiated

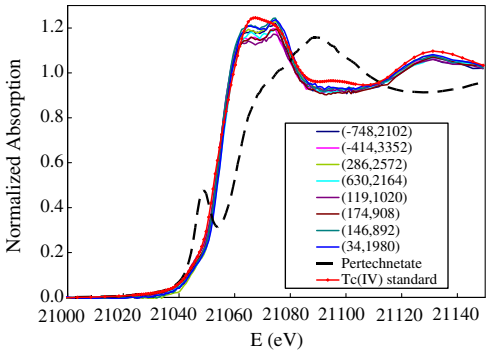

Fig. 7. Micro-XANES analysis of Tc-valence in 8-Tc hot spots in a 60 μm thin section of oxidized, water-extracted FRC sediment. The labels refer to the locations of the particles (see the Electronic Annex for the corresponding images).

(Fig. 8). Discrete particles with intense co-incident signals of all three elements were represented by particle #7. Discrete particles with spatially variable Rb, and coincident Fe and Tc were represented by particle #15. Smaller/thinner particle aggregates with lower Tc concentration were represented by particle #13. Clearly, these were all variants on a common geochemical theme. The relative concentration intensities for Tc and Fe within each pixel of each particle were quantified from the XRM images. These two variables showed good correlation for many particles, with oxidation-resistant Tc concentration increasing with associated Fe concentration (Fig. 9). The correlation structure implied the presence of three types of Fe-containing zones within the measured particles, including those with low, intermediate, and high potential to stabilize Tc(IV). All of the points with Tc intensity > 0.4 in Fig. 9 were from parti-

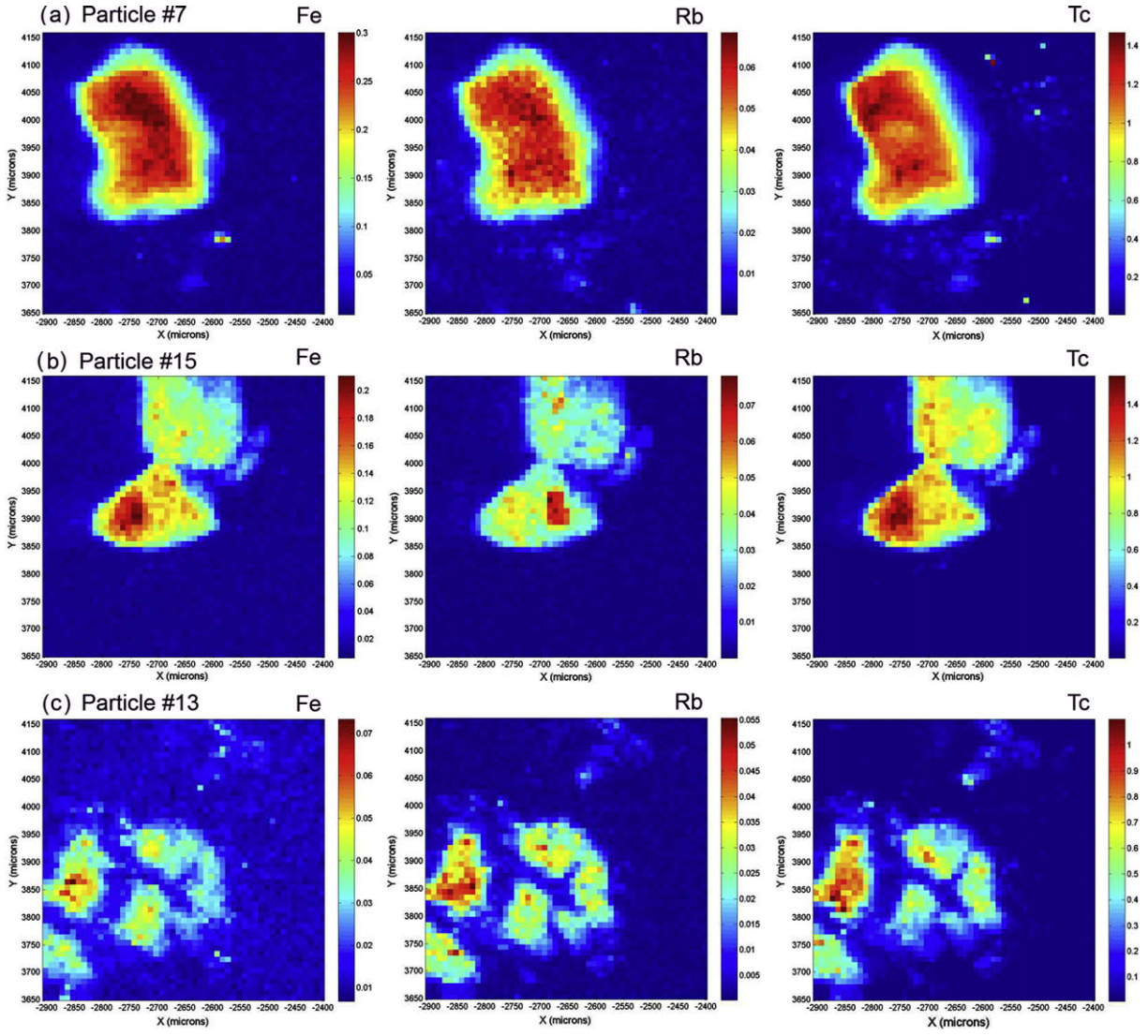

Fig. 8. X-ray microprobe (XRM) chemical distribution maps for three representative types of Tc-containing particles isolated from oxidized FRC sediment. Fluorescence intensity maps are shown for the noted particles for Tc, Fe, and Rb, with red denoting the highest signal (proportional to elemental concentration). Rb is a chemical surrogate for K. (For interpretation of the references to color in this figure legend, the reader is referred to the web version of this paper.)

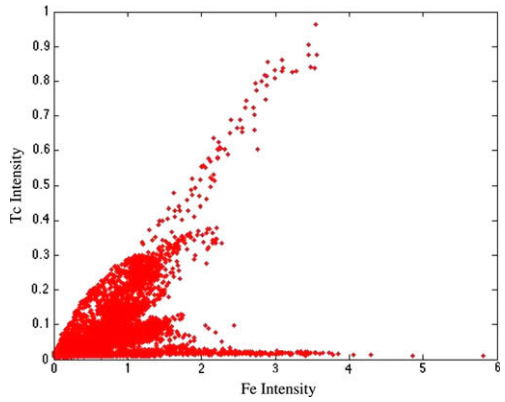

Fig. 9. XRM concentration intensity of Fe and Tc for all isolated Tc-containing particles from oxidized, water-washed FRC sediment. Concentration intensities calculated from single pixels in each particle containing high-Tc. Particle #7 had particularly high Fe and Tc concentrations that are noted.

cle #7, where many pixels within this grain displayed uniform correlation between Fe and Tc regardless of their spatial location.

Electron microprobe backscattered electron imaging of particle morphology (Fig. 10a) and chemical analysis (Fig. 10b) of example particle #7 were consistent with the Tc(IV)-bearing particles being Fe-containing micas in various stages of weathering. Iron containing micas of comparable dimension and composition were previously observed in porous weathered clasts of the FRC sediment [Fig. 1b in Kukkadapu et al. (2006)]. Tc spatial distribution did not show obvious correlation with morphologic features of the particle, but there was some evidence that oxidation-resistant Tc was concentrated (dark-red[1]) near basal plane edge steps or corrugated edge features (upper right, Fig. 10c). Each of these locations is an entry point to mica interlaminar space where diffusionally restricted domains occur. Hot spots at the lower left show no apparent morphologic relationship.

Micro-EXAFS of good quality was collected on five of the particles (Fig. 11, see Electronic Annex Fig. EA-1-6 for the $\chi(k)$ data). The FT-spectra were similar for five of the particles and dissimilar for the sixth (particle #13). The common spectra observed for the four samples was different from that of the initial redox product (Fig. 6), but similar to that for heterogeneously reduced Tc on Fe(III) oxide surfaces with sorbed Fe(II) (Zachara et al., 2007b; Peretyazhko et al., 2008a). The small peak at 2.3 Å is characteristic of a predominance of Fe(III) in the second coordination shell of Tc(IV) implying that the average Tc–Tc chain length was small (less than 2). All of these spectra [heterogeneous Tc on Fe(III) oxides and the five common sediment particles resistant to oxidation] were well described with a model containing adsorbed octahedral monomers and dimers of TcO_2 that were complexed in edge-sharing fashion to Fe(III)–O octahedra. The dissimilar spectra for particle #13 implied significant disorder in the second coordination sphere and beyond.

Four of the five particles in Fig. 11 were successfully transferred to a sample mount for single particle, micro-XRD analyses. Three of these yielded interpretable diffraction patterns (Fig. 12). Two of the particles (#7 and #11) exhibited reflections consistent with the 1 M mica polytype of celadonite. Celadonite is a dioctahedral Fe(III)–mica of ideal composition $KMgFe^{3+}Si_4O_{10}(OH)_2$ with Fe(III) occupying octahedral sites (Odom, 1987). It is an end-member in the muscovite-celadonite series of true K micas that display considerable solid-solution behavior involving Mg^{2+}, Al^{3+}, and Fe(III)/Fe(II) (Li et al., 1997; Tischendorf et al., 2007). The diffraction pattern for the third particle (#27) was less conclusive, but it also appeared to contain some celadonite as well as quartz and possibly muscovite. Quartz was a dominant mineral phase associated with Fe-micas in weathered FRC clasts (Kukkadapu et al., 2006). Residual crystalline graphitic carbon from EMP analysis was also evident in the particle XRD patterns.

All three of these particles exhibited common EXAFS spectra for the apparently oxidation-resistant Tc(IV) (Fig. 11), implying that celadonite might be the stabilizing mineral phase. Celadonites also contain significant Rb (Booij et al., 1995; Innocent et al., 1997), an element that was consistently found in association with oxidation-resistant Tc(IV) (Fig. 8). The presumptive identification of celadonite in particle #7 by XRD was fully consistent with: (i) the EMP analyses (Fig. 10b), as Al and other ion substitutions are common and extensive in celadonites as they are in other micas (Weaver and Pollard, 1975; Li et al., 1997; Tischendorf et al., 2007), and (ii) ^{57}Fe Mössbauer analyses of the FRC sediment indicating presence of Fe(III)/Fe(II)-containing phyllosilicates (Kukkadapu et al., 2006).

4. DISCUSSION

4.1. TcO_4^- reduction in FRC vs. Ringold sediment

The Ringold and FRC materials both exhibited substantial capacities for biogenic Fe(II)-facilitated TcO_4^- reduction but varied considerably with regard to the rate at which the consecutive spikes of TcO_4^- were reduced (Fig. 2). This result was in direct contrast to the relative concentrations of 0.5 N HCl-extractable Fe(II) in the two sediments, 12 and 5.4 mM for the FRC and Ringold materials, respectively. The results were consistent, however, with previous observations that 20 μM TcO_4^- was reduced more rapidly in the Ringold relative to the FRC saprolite even when the Ringold sediment contained significantly lower concentrations of HCl-extractable Fe(II) (Fredrickson et al., 2004). Our initial interpretation of this result was that the FRC saprolite has an abundance of Fe-containing layer silicates including mica, illite, vermiculite, and smectite; and that the Fe(II) associated with these phases was kinetically slower to react with TcO_4^- than Fe(II) sorbed to Fe(III) oxides coating quartz grains in Ringold sediment. The slow redox reactivity of the FRC phyllosilicate fraction, relative to goethite and hematite with adsorbed Fe(II), has been recently demonstrated

[1] For interpretation of the references to color in Fig. 10, the reader is referred to the web version of this paper.

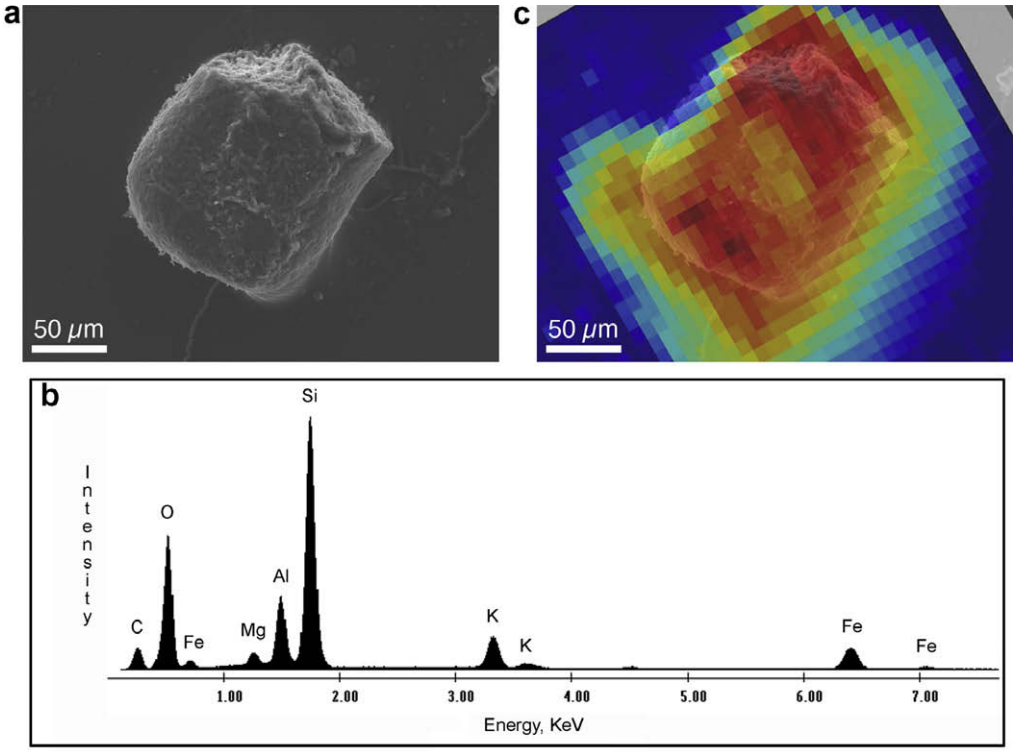

Fig. 10. Characterization of Tc-containing particle #7 isolated from oxidized FRC sediment: (a) backscattered electron (BSE) micrograph, (b) electron microprobe EDS analysis, and (c) BSE image with XRM, Tc-concentration overlay.

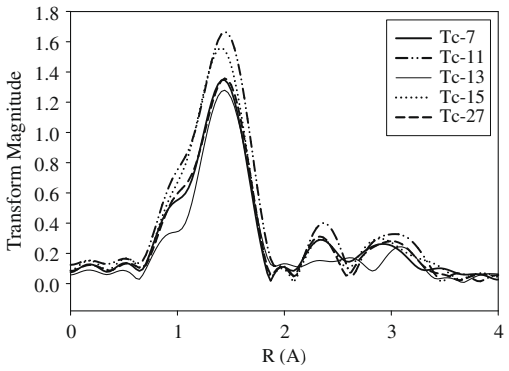

Fig. 11. Technetium micro-EXAFS analysis (FT spectra) of Tc-containing particles #7, 11, 13, 15, and 27 isolated from oxidized, water-washed oxidized FRC sediment.

(Peretyazhko et al., 2008a). However, the molecular speciation of heterogeneous Tc(IV) in both sediments was identical, and more similar to that observed for heterogeneous Tc on phyllosilicate and Al-oxide surfaces, rather than Fe(III) oxides (Peretyazhko et al., 2008a,b). It was not resolved whether this common speciation was due to the same reduction mechanism, or to the use of significantly higher (e.g., 10×) Tc(VII) concentrations in comparison to the previous studies. In addition, the FRC saprolite is comprised of sand and silt-sized aggregates consisting of clay and silt-sized particles that were variably cemented. Based on these characteristics we also postulated that the slower rates of TcO_4^- reduction may have been due to intra-aggregate diffusion of TcO_4^- into regions that were sufficiently high in Fe(II) to facilitate electron transfer from Fe(II) and subsequent reduction of Tc(VII) to Tc(IV).

Backscattered electron imaging and electron microprobe analyses of the <2.0-mm fraction of the FRC saprolite revealed two distinct clast types: one containing relatively larger crystallites with significant "sponge-like" internal pore space and 50–100 μm Fe-containing micas; and a second type that was more compact with limited internal porosity, very small crystallites, and a significant Fe mass (average 6.12 wt%; Kukkadapu et al., 2006). Anoxic incubation of the FRC sediment with electron donor and CN32 reduced approximately 10–15% of $Fe(III)_{TOT}$, with reduction being equally distributed between the phyllosilicate and goethite fractions. Fe(II) resulting from bioreduction remained in a layer silicate environment that exhibited enhanced solubility in weak acid, and as a discrete, unidentified biotransformation product of goethite. These results indicated that *S. putrefaciens* CN32, the same organism used in the current experiments, was able to reduce intra-aggregate Fe(III). In the experiments presented herein, conducted under essentially identical conditions as the previous study (Kukkadapu et al., 2006), biogenic Fe(II) would have been present in both types of clasts. The intrinsic reactivity of these two classes of biogenic Fe(II) with regard to the heterogeneous reduction of Tc(VII) is unknown.

Although we believe that mineralogically-controlled differences existed in the intrinsic reactivity of biogenic Fe(II) in the two sediments, we also suggest that the slow (~100 d)

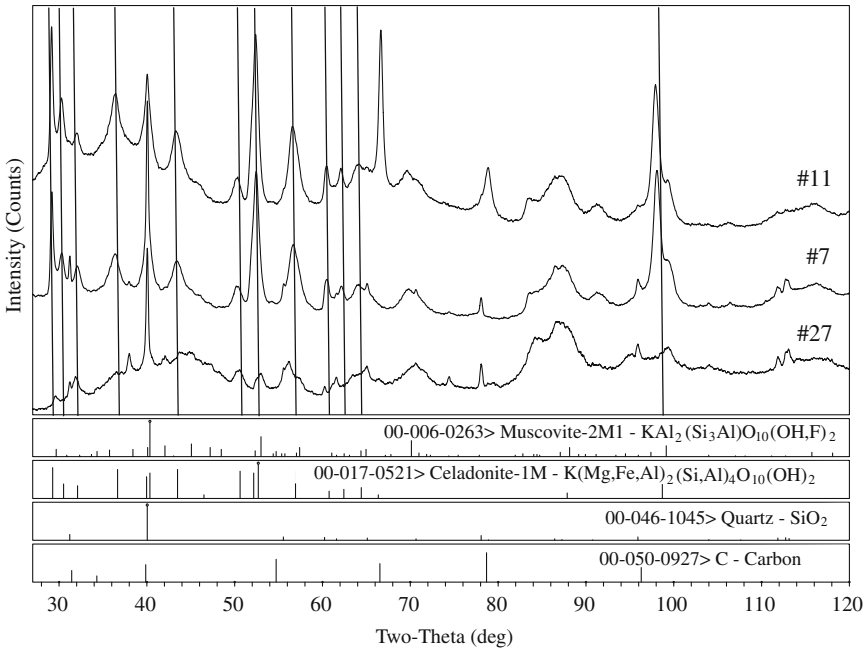

Fig. 12. Micro X-ray diffraction analyses of three individual sediments particles exhibiting air oxidation-resistant Tc(IV).

rate of reduction observed upon the third spike (1.25 mM) of TcO_4^- into the FRC saprolite, relative to the Ringold sediment (~12 d), resulted from slow mass transfer of TcO_4^- into compact aggregates. As the initial and more physically accessible Fe(II) is oxidized by TcO_4^-, the remaining reactive Fe(II) is likely to be associated with aggregate interiors. Consequently, the distance for diffusion, and hence the extended time require for Tc(VII) reduction, becomes increasingly longer as the readily accessible Fe(II) is depleted.

4.2. Biogenic and abiogenic Tc(IV) susceptibility to oxidative solubilization

In the absence of sediment, biogenic $TcO_2{\cdot}nH_2O_{(s)}$ is rapidly oxidized in air to TcO_4^-, as would be expected based on thermodynamic considerations. In unreduced Ringold and FRC sediment biogenic $TcO_2{\cdot}nH_2O_{(s)}$ is also oxidized to TcO_4^-, but as these experiments were conducted in the absence of air, O_2 could not have been the oxidant. As the Ringold sediment contains an appreciable concentration of NH_2OH–HCl extractable Mn (171 μmol/g), mainly as todorokite $Na_{0.2}Ca_{0.05}K_{0.02}Mn_4^{4+}Mn_2^{3+}O_{12} \cdot 3(H_2O)$ (Zachara et al., 1995; Fredrickson et al., 2002), it is likely that this Mn(III/IV) phyllomanganate was the oxidant. It is well established that Mn oxides are effective oxidants of organic compounds (Stone and Morgan, 1984) and reduced metals such as uraninite (UO_2) (Fredrickson et al., 2002) and Co(II)-EDTA complexes (Zachara et al., 1995). In previous investigations, 20 μM biogenic $TcO_2{\cdot}nH_2O_{(s)}$ was oxidized in anoxic but unreduced FRC saprolite, and an unidentified Mn(III/IV) oxide component (33.2 μmol/g of NH_2OH–HCl extractable Mn) was similarly implicated (Fredrickson et al., 2002). Herein, we investigated the capacity for the Mn oxide fraction of the FRC saprolite to oxidize biogenic $TcO_2{\cdot}nH_2O_{(s)}$ and although extensive oxidation was observed, it was less than predicted based on the stoichiometric reaction of Mn(III/IV) with the added TcO_2. For these experiments, the sediments were continuously mixed (shaking at 25 rpm), a factor that likely facilitated the reaction between $TcO_2{\cdot}nH_2O_{(s)}$ and the Mn oxides, both solid phases. In the absence of mixing, there would have been limited contact between these solids and hence, the kinetics of oxidation likely would have been much slower and potentially less extensive. Additionally, available surface area and accessibility of the Mn oxide component could have been an important factor limiting the oxidation of the $TcO_2{\cdot}nH_2O_{(s)}$ in the FRC saprolite. For example, if Mn is distributed among both the weathered and compact clast types in the FRC saprolite, Mn oxide residing in the interior of the compact clasts would have been inaccessible to $TcO_2{\cdot}nH_2O_{(s)}$. X-ray microprobe analytical transects revealed a relatively equal Mn abundance between the two clast types (data not shown), and hence approximately one-half of the Mn would have been distributed in the compact fraction and likely unable to come in physical contact with the exogenously added $TcO_2{\cdot}nH_2O_{(s)}$.

The rapid kinetics of TcO_4^- reduction observed in the bioreduced Ringold sediment relative to the FRC saprolite were also observed during the reverse (oxidation) reaction, albeit at slower rates (Table 1). There was little resistance to air oxidation of the Tc(IV) phase in the Ringold sediment. At the same concentration (1000 μM), sediment-associated Tc(IV) was oxidized by air at an equivalent rate to biogenic $TcO_2{\cdot}nH_2O_{(s)}$ in the absence of sediment (Table 1), with all product $Tc(VII)O_4^-$ released quantitatively to the aqueous phase. This suggests that Tc reduced by the Ringold biogenic Fe(II) was readily accessible to dissolved O_2.

In contrast to the Ringold sediment, oxidative solubilization of the Tc(IV) phase was slow and incomplete in the FRC sediment (Figs. 3a and 4b and Table 1). Differences in redox product speciation could not be the cause, as speciation was apparently the same in both sediments (Fig. 6). In a microcosm study also using sediments from the FRC background site, 0.5 μM Tc(VII) was removed from solution under Fe(III)-reducing conditions with hydrous TcO_2 as the predominant reduction product (McBeth et al., 2007). Although the mechanism of reduction was not directly established, i.e., direct enzymatic vs. indirect via biogenic Fe(II), Tc(VII) reduction did not commence until the onset of Fe(III) reduction. McBeth et al. (2007) and Morris et al. (2008) also observed significant (~80%) remobilization of Tc from reduced FRC sediment to solution upon air oxidation, comparable to the ~75% remobilization of Tc upon air oxidation observed in this study. It is possible that a Fe-containing mica fraction in the FRC sediment in the cited studies may have been responsible for the observed Tc(IV) air oxidation-resistance, similar to the observations reported herein. Burke et al. (2006) observed in estuarine sediment that ~50% of reduced Tc was remobilized to solution as TcO_4^-. Their EXAFS analyses indicated that the air-oxidized sediment contained a mixture of Tc(IV), as $TcO_2{\cdot}nH_2O$, and Tc(VII), as TcO_4^-. We observed a similar result with the FRC saprolite, in which ~25% of the sorbed/reduced Tc remained associated with the solid phase even after extensive air oxidation. XANES analyses of the unwashed sediment after oxidation yielded a mixed distribution of Tc(IV) and Tc(VII) similar to that observed by Burke et al. Extensive water extraction of the oxidized sediment removed soluble Tc(VII), leaving a stable, oxidation-resistant sorbed Tc(IV) phase. We therefore concluded that mass transfer limitations slowing O_2 ingress into compact aggregates, and the formation of a stable, Tc(IV) phase, possibly in association with Fe(III) oxidation products, caused the noted differences in FRC oxidation behavior in comparison to the RG sediment.

4.3. Factors contributing to TcO_2 resistance to air oxidation in FRC sediment

In experiments where TcO_4^- was reduced by structural Fe(II) associated with subsurface fracture fill containing granite, hornblende and magnetite and then exposed to air-saturated groundwater, the oxidative release of Tc into solution over a 3 week period was very slow (Cui and Eriksen, 1996). It was suggested that competing reaction between mineral-associated Fe(II) and O_2 suppressed Tc(IV) oxidation. In our experiments with the Ringold sediment, there was an initial rapid oxidation of Fe(II) followed by what appeared to be a much slower oxidation phase. Although the sparse sample points do not allow precise determination of Fe(II) oxidation relative to Tc, it is possible that residual Fe(II) may have provided some buffering against O_2 oxidation of Tc(IV) in the FRC saprolite.

Residual Tc(IV) that was recalcitrant to oxidation in the FRC sediment was clearly evident as 25–100-μm hot spots by XRM. Recalcitrant Tc(IV) appeared to concentrate in association with Fe and Rb (a proxy for K), and to mimic their spatial distribution. The size, morphology, and chemical composition of the host mineral phases suggested that they were Fe-containing micas. Moreover, the isolation and analysis of Tc-containing mineral particle micas indicated a structure and chemical composition consistent with celadonite, a relatively uncommon mica form typically associated with oceanic and continental basalts (Innocent et al., 1997; Li et al., 1997). Celadonite can exist as a detrital phase in sediments derived from these sources (Odom, 1987). The Fe(III)/Fe(II) ratio of the FRC celadonite was not directly determined, but ^{57}Fe Mössbauer measurements indicated that the FRC micaceous fraction (specific phases undetermined) contained both Fe(II) and Fe(III) (Kukkadapu et al., 2006). Comparable Fe-containing micas were not evident in the specific Hanford Ringold sediment studied in spite of its sizable content of lithic fragments of continental flood basalt origin; instead, muscovite was dominant with lessor amounts of biotite (Zachara et al., 1995; Fredrickson et al., 2004). Celadonite can weather to Fe-rich smectite (Reid et al., 1988), and mineralogic studies of the FRC sediment found a sizable content of Fe–phyllosilicates in the <2.0 μm clay fraction (Kukkadapu et al., 2006).

Tc(IV) was observed through cross sections of the host mica by XRM and not simply along their periphery as would occur if they were surface precipitates. However, details of the internal Tc(IV) elemental and structural association were not evident given the XRM measurement scale. Presumptive evidence was observed in certain cases for diffusion-controlled profiles where Tc appeared depleted around particle peripheries, and enriched in interiors. The Fe(III)/Fe(II)-containing micas present in the FRC saprolite (now presumed to be celadonite) have persisted over long periods of oxidative weathering (Kukkadapu et al., 2006). Consistent with their apparent limited reactivity toward O_2, the Fe-micas do not exhibit heterogeneous redox reactivity toward Tc(VII) in the absence of bioreduction (Fredrickson et al., 2004; Peretyazhko et al., 2008a). The DCB-treated phyllosilicate fraction of the FRC sediment (including the 50–100 μm mica fraction and clay-sized phyllosilicates) heterogeneously reduces Tc(VII) (Peretyazhko et al., 2008a). This reactivity, however, was attributed to reductive genesis of Fe(II)-containing phyllosilicates in the clay-sized fraction, and not to the coarser-textured micas whose Mössbauer spectra were unchanged with either reduction or oxidation (Peretyazhko et al., 2008a).

It is not clear why the large particle Fe-micas or celadonites host oxidation-stable Tc(IV). Tc(IV) is remarkably stable in these phases, resisting oxidation for over one year in contact with air. EXAFS measurements of the recalcitrant Tc(IV) indicated that it was associated with octahedral Fe(III) within the Fe-mica. The EXAFS spectra were similar to heterogeneously reduced/precipitated Tc(IV) resulting from reaction with Fe(II)-sorbed goethite, hematite, and ferrihydrite (Zachara et al., 2007b; Peretyazhko et al., 2008a). Whether this Fe(III) was a structural constituent in the octahedral layer of celadonite, or nanoparticulate Fe(III) oxide resulting from in-situ weathering, or oxidation following laboratory bioreduction, was not determined by our analysis. This Tc(IV)–Fe(III) molecular speci-

ation form oxidizes more slowly and less extensively than either biogenic or abiotic $TcO_2{\cdot}nH_2O$ (Zachara et al., 2007b). Perhaps Tc(IV) at the end of TcO_2 chains is more readily oxidized than Tc(IV) directly bonded to Fe–O octahedral sites. Oxidation resistance of Tc(IV) appears to result from short chain length.

It was not resolved whether the recalcitrant Tc(IV)–Fe(III) association or phase was an initial minor redox product that was masked in EXAFS by larger concentrations of the TcO_2-like phase, or an oxidation-induced transformation product. The experimental evidence suggests that oxidation-recalcitrant Tc(IV) was generated by Tc(VII) reaction with celadonite-associated Fe(II) generated through bioreduction of octahedral Fe(III) sites. Further mechanistic details on the formation of this molecular association and the nature of its surrounding structural environment that inhibits oxidation are unknown and require additional study. Nonetheless, it appears that a complex transformation involving Tc(IV), Fe(II), and Fe(III) in physically restricted interlamellar space of Fe-mica is responsible for the unexpected long-term stability of the Tc(IV) mineral association. It is curious and remains unexplained, why similar oxidation-resistant micaceous phase associations did not form in the Ringold sediment, as this sediment contains a diverse mica fraction derived from basaltic and granitic sources (Fredrickson et al., 2004). Mössbauer analyses, however, indicate that the FRC micas contain more Fe than do those in the Ringold (Fredrickson et al., 2004; Kukkadapu et al., 2006), and this appears to be the key variable inhibiting Tc(IV) oxidation.

5. ENVIRONMENTAL IMPLICATIONS

At DOE's Hanford Site, where it is a contaminant of major concern, ^{99}Tc has migrated to significant depths in the vadose zone which, in the central plateau area of Hanford, is close to 60 m. Experiments with contaminated vadose zone sediments collected beneath tank T-106 at Hanford (that released 2.11 Ci of ^{99}Tc) indicate that ^{99}Tc is freely mobile (RPP, 2005), yielding aqueous concentrations of >15 μmol/L (~2.0×10^7 pCi/L) in contacting porewater. Larger in-ground inventories of ^{99}Tc exist within Hanford's S-SX tank farm [~30 Ci; Khaleel et al. (2007)] and the BC cribs [410 Ci; Serne and Mann, 2004; Kincaid et al., 2006; Rucker and Fink, 2007]. In the absence of barriers to prevent infiltration or as yet untried deep vadose zone remediation techniques, there is little to prevent this mobile ^{99}Tc from eventually entering Hanford's unconfined aquifer and traveling with groundwater that to the Columbia River. Contamination of the Columbia River by ^{99}Tc represents a serious concern as the drinking water standard is low (900 pCi/L or $<10^{-9}$ mol/L). At Hanford's Waste Management Area T, ^{99}Tc has already entered the groundwater, yielding concentrations of 182,000 pCi/L at 10 m below the water table (Hartman et al., 2006).

The in situ reduction of TcO_4^- to poorly soluble Tc(IV) in the subsurface is a potential means for limiting the migration of ^{99}Tc into surface waters. For example, the in situ stimulation of an extant subsurface microbial community at DOE's Oak Ridge site was achieved by the injection of electron donor (acetate, ethanol or glucose) resulting in the reduction of TcO_4^-, with consequent immobilization, that occurred concurrently with NO_3^- utilization (Istok et al., 2004). While these results demonstrate the feasibility of in situ stimulation of TcO_4^- reduction, the experiment was performed at shallow depth and over a relatively small area. The practicality and efficacy of achieving a sufficiently extensive in situ stimulation of the subsurface microbial community at a scale and depth that would be required at Hanford to be impactful is questionable. The unconfined aquifer at Hanford is oligotrophic and limited measurements suggest that subsurface microbial populations are sparse (Kieft et al., 1995); increasing the size of the biomass and sustaining activity over an extended area would be technically challenging and costly.

It is currently unclear whether localized anoxic regions exist, at either macroscopic or microscopic scales, within the Hanford unconfined aquifer, which reaches over 30 m in thickness in certain locations and exhibits considerable heterogeneity in hydrogeologic properties. Aqueous and sorbed ferrous iron could be generated by low but sustained microbial activities and/or the weathering of Fe(II)-bearing minerals present such as Fe(II)–basaltic glass, pyroxene, ilmenite/magnetite, or chlorite/lizardite (Zachara et al., 2007c) in restricted environments to favor heterogeneous Tc(VII) reduction. Over 60% of the sizable total Fe concentration in Hanford sediment exists as structural Fe(II), underscoring the plausibility of such reactions. US Atlantic coastal plain sediments that were naturally anoxic with Fe(II) concentrations exceeding a ratio of 4.3 Fe(II):Tc(-VII) (TcO_4^- added at concentrations of 1–2.5 μmol g dry wt. sediment) exhibited relatively rapid reduction to $TcO_2{\cdot}nH_2O_{(s)}$ (Wildung et al., 2004), demonstrating the feasibility of intrinsic Tc(VII) reduction. Given the low total concentration of contaminant Tc Hanford pore- and groundwaters (10^{-8}–10^{-5} mol/L); a relatively small amount of soluble/sorbed Fe(II) could have a profound effect on Tc valence speciation and effective solubility.

Regardless of whether Tc solubility is reduced via direct microbial reduction or indirectly by adsorbed Fe(II), the susceptibility of $TcO_2{\cdot}nH_2O_{(s)}$ to oxidation by O_2 remains a concern for long-term stability. In shallow or deep subsurface environments that are naturally oxic and require either stimulation of microbial activity or treatment with a chemical reductant such as dithionite (Fruchter et al., 2000) to achieve sufficient Fe(II) concentrations to facilitate Tc(VII) reduction, the treated zone must remain anoxic to prevent re-mobilization of Tc(IV) via oxidation by O_2. However, as observed herein, there may be situations where sediment physical properties, Fe mineralogy, or the chemical nature of Tc or Tc–Fe molecular interactions during reduction–oxidation processes limit or prevent mobilization into groundwater. The findings presented herein indicate that certain forms and/or locations of Tc(IV) generated via reduction by sediment-associated Fe(II), especially Fe in association with phyllosilicates, may be exceedingly resistant to oxidative remobilization. These processes may have a significant impact on the long-term fate and transport of Tc in the subsurface at locations such as Hanford but remain poorly understood. Their understanding will be

critical for ensuring the long-term immobilization of Tc in the subsurface to impede or prevent its mobility in the subsurface and contamination of surface waters such as the Columbia River.

ACKNOWLEDGMENTS

We wish to thank Tom Resch for preparation of samples for XAS analysis. This research was supported by the Environmental Remediation Science Program (ERSP), Office of Biological and Environmental Research (OBER), US Department of Energy (DOE). PNC/XOR facilities at the Advanced Photon Source, and research at these facilities, are supported by the US Department of Energy – Basic Energy Sciences, a major facilities access grant from NSERC, the University of Washington, Simon Fraser University and the Advanced Photon Source. Use of the Advanced Photon Source is also supported by the US Department of Energy, Office of Science, Office of Basic Energy Sciences, under Contract DE-AC02-06CH11357. Mössbauer analyses and micro X-ray diffraction were performed using EMSL, a national scientific user facility sponsored by the Department of Energy's Office of Biological and Environmental Research located at Pacific Northwest National Laboratory. We thank Dr. Ravi Kukkadapu for performing the Mössbauer analysis and modeling. PNNL is operated for the Department of Energy by Battelle.

APPENDIX A. SUPPLEMENTARY DATA

Supplementary data associated with this article can be found, in the online version, at doi:10.1016/j.gca.2009.01.027.

REFERENCES

Booij E., Gallahan W. E. and Staudigel H. (1995) Ion-exchange experiments and Rb/Sr dating on celadonites from the Troodos ophiolite, Cyprus. *Chem. Geol.* **126**, 155–167.

Burke I. T., Boothman C., Lloyd J. R., Mortimer R. J. G., Livens F. R. and Morris K. (2005) Effects of progressive anoxia on the solubility of technetium in sediments. *Environ. Sci. Technol.* **39**, 4109–4116.

Burke I. T., Boothman C., Lloyd J. R., Livens F. R., Charnock J. M., McBeth J. M., Mortimer R. J. G. and Morris K. (2006) Reoxidation behavior of technetium, iron, and sulfur in estuarine sediments. *Environ. Sci. Technol.* **40**, 3529–3535.

Chao T. T. (1972) Selective dissolution of manganese oxides from soils and sediments with acidified hydroxylamine hydrochloride. *Soil Sci. Soc. Am. Proc.* **36**, 764–768.

Cui D. and Eriksen T. E. (1996) Reduction of pertechnetate by ferrous iron in solution: influence of sorbed and precipitated Fe(II). *Environ. Sci. Technol.* **30**, 2259–2262.

Evans J. C., Dresel P. E. and Farmer O. T. (2007) Inductively coupled plasma, mass spectrometric isotopic determination of nuclear wastes sources associated with Hanford tank leaks. *Vadose Zone J.* **64**, 1042–1049.

Fredrickson J. K., Zachara J. M., Kennedy D. W., Dong H., Onstott T. C., Hinman N. W. and Li S. W. (1998) Biogenic iron mineralization accompanying the dissimilatory reduction of hydrous ferric oxide by a groundwater bacterium. *Geochim. Cosmochim. Acta* **62**, 3239–3257.

Fredrickson J. K., Zachara J. M., Kennedy D. W., Liu C., Duff M. C., Hunter D. B. and Dohnalkova A. (2002) Influence of Mn oxides on the reduction of uranium(VI) by the metal-reducing bacterium *Shewanella putrefaciens*. *Geochim. Cosmochim. Acta* **66**, 3247–3262.

Fredrickson J. K., Zachara J. M., Kennedy D. W., Kukkadapu R. K., McKinley J. P., Heald S. M., Liu C. and Plymale A. E. (2004) Reduction of TcO_4^- by sediment-associated biogenic Fe(II). *Geochim. Cosmochim. Acta* **68**, 3171–3187.

Fruchter J. S., Cole C. R., Williams M. D., Vermeul V. R., Amonette J. E., Szecsody J. E., Istok J. D. and Humphrey M. D. (2000) Creation of a subsurface permeable treatment zone for aqueous chromate contamination using in situ redox manipulation. *Ground Water Monitor. Remed.* **20**, 66–77.

Gambrell R. P. (1996) Manganese in methods of soil analysis. Part 3. In *Chemical Methods* (ed. D. L. Sparks). Soil Science Society of American and American Society of Agronomy, Madison, WI.

Gee G. W., Oostrom M., Freshley M. D., Rockhold M. L. and Zachara J. M. (2007) Special section: Hanford Site. *Vadose Zone J.* **64**, 899–1056.

Hartman M. J., Morasch L. F. and Webber W. D. (2006) Summary of Hanford Site Groundwater Monitoring for Fiscal Year 2005. Pacific Northwest National Laboratory, Richland, WA.

Heron G., Bjerg P. L. and Christensen T. H. (1995) Redox buffering in shallow aquifers contaminated by leachate. In *Intrinsic Bioremediation* (eds. R. E. T. W. J. Hinchee and D. C. Downey). Battelle Press, Columbus, OH.

Innocent C., Parron C. and Hamelin B. (1997) Rb/Sr chronology and crystal chemistry of celadonites from the Parana continental tholeiites, Brazil. *Geochim. Cosmochim. Acta* **61**, 3753–3761.

Istok J. D., Senko J. M., Krumholz L. R., Watson D., Bogle M. A., Peacock A., Chang Y. J. and White D. C. (2004) In situ bioreduction of technetium and uranium in a nitrate-contaminated aquifer. *Environ. Sci. Technol.* **38**, 468–475.

Khaleel R., White M. D., Oostrom M., Wood M. I., Mann F. M. and Kristofzski J. G. (2007) Impact assessment of existing vadose zone contamination at the Hanford Site SX tank farm. *Vadose Zone J.* **64**, 935–945.

Kieft T. L., Fredrickson J. K., McKinley J. P., Bjornstad B. N., Rawson S. A., Phelps T. J., Brockman F. J. and Pfiffner S. M. (1995) Microbiological comparisons within and across contiguous lacustrine, paleosol, and fluvial subsurface sediments. *Appl. Environ. Microbiol.* **61**, 749–757.

Kincaid C. T., Eslinger P. W., Aaberg R. L., Miley T. B., Nelson I. C., Strenge D. L. and Evans J. C. (2006). Inventory Data Package for Hanford Assessments. *PNNL-15829*, Pacific Northwest National Laboratory, Richland, WA.

Komlos J., Kukkadapu R. K., Zachara J. M. and Jaffe P. R. (2007) Biostimulation of iron reduction and subsequent oxidation of sediment containing Fe-silicates and Fe-oxides: effect of redox cycling on Fe(III) bioreduction. *Water Resour.* **41**, 2996–3004.

Kukkadapu R. K., Zachara J. M., Fredrickson J. K., McKinley J. P., Kennedy D. W., Smith S. C. and Dong H. (2006) Reductive biotransformation of Fe in shale-limestone saprolite containing Fe(III) oxides and Fe(II)/Fe(III) phyllosilicates. *Geochim. Cosmochim. Acta* **70**, 3662–3676.

Li G., Peacor D. R., Coombs D. S. and Kawachi Y. (1997) Solid solution in the celadonite family: the new minerals ferroceladonite, $K_2Fe_2^{2+}Fe_2^{3+}Si_8O_{20}(OH_4)$, and ferroaluminoceladonite, $K_2Fe_2^{2+}Al_2Si_8O_{20}(OH_4)$. *Am. Mineral.* **82**, 503–511.

Liu D. J., Yao J., Wang B., Bruggeman C. and Maes N. (2007) Solubility study of Tc(IV) in a granitic water. *Radiochim. Acta* **95**, 523–528.

Lloyd J. R. and Macaskie L. E. (1996) A novel phosphorimager-based technique for monitoring the microbial reduction of technetium. *Appl. Environ. Microbiol.* **62**, 578–582.

Lloyd J. R., Cole J. A. and Macaskie L. E. (1997) Reduction and removal of heptavalent technetium from solution by *Escherichia coli*. *J. Bacteriol.* **179**, 2014–2021.

Lloyd J. R., Ridley J., Khizniak T., Lyalikova N. N. and Macaskie L. E. (1999) Reduction of technetium by *Desulfovibrio desulfuricans*: biocatalyst characterization and use in a flowthrough bioreactor. *Appl. Environ. Microbiol.* **65**, 2691–2696.

Lloyd J. R., Sole V. A., Van Praagh C. V. G. and Lovley D. R. (2000) Direct and Fe(II)-mediated reduction of technetium by Fe(III)-reducing bacteria. *Appl. Environ. Microbiol.* **66**, 3743–3749.

Lukens, Jr., W. W., Bucher J. J., Edelstein N. M. and Shuh D. K. (2002) Products of pertechnetate radiolysis in highly alkaline solution: structure of TcO_2xH_2O. *Environ. Sci. Technol.* **36**, 1124–1129.

Marshall M. J., Plymale A. E., Kennedy D. W., Wang Z., Reed S. B., Dohnalkova A. C., Simonson C. J., Liu C., Saffarini D. A., Romine M. F., Zachara J. M., Beliaev A. S. and Fredrickson J. K. (2008) Hydrogenase- and outer membrane c-type cytochrome-facilitated reduction of technetium(VII) by *Shewanella oneidensis* MR-1. *Environ. Microbiol.* **10**, 125–136.

Marshall M. J., Dohnalkova A. C., Kennedy D. W., Plymale A. E., Thomas S. H., Löffler F. E., Sanford R. A., Zachara J. M., Fredrickson J. K. and Beliaev A. S. (2009) Electron donor dependent radionuclide reduction and nanoparticle formation by *Anaeromyxobacter dehalogenans* strain 2CP-C. *Environ. Microbiol.* **11**, 534–543.

McBeth J. M., Lear G., Lloyd J. R., Livens F. R., Morris K. and Burke I. T. (2007) Technetium reduction and reoxidation in aquifer sediments. *Geomicrobiol. J.* **24**, 189–197.

Morris K., Livens F. R., Charnock J. M., Burke I. T., McBeth J. M., Begg J. D. C., Boothman C. and Lloyd J. R. (2008) An X-ray absorption study of the fate of technetium in reduced and reoxidized sediments and mineral phases. *Appl. Geochem.* **23**, 603–617.

Odom I. E. (1987) Glauconite and celadonite minerals. In *Reviews in Mineralogy* (ed. S. W. Bailey). Mineralogical Society of America.

Peretyazhko T., Zachara J. M., Heald S. M., Jeon B. H., Kukkadapu R. K., Liu C., Moore D. and Resch C. T. (2008a) Heterogeneous reduction of Tc(VII) by Fe(II) at the solid–water interface. *Geochim. Cosmochim. Acta* **72**, 1521–1539.

Peretyazhko T., Zachara J. M., Heald S. M., Kukkadapu R. K., Liu C., Plymale A. E. and Resch C. T. (2008b) Reduction of Tc(VII) by Fe(II) sorbed on Al (hydro)oxides. *Environ. Sci. Technol.* **42**, 5499–5506.

Reid D. A., Graham R. C., Edinger S. B., Bowen L. H. and Ervin J. O. (1988) Celadonite and it's transformation to smectite in an entisol at Red Rock Canyon, Kern County, California. *Clays Clay Miner.* **36**, 425–431.

Riley R. G. and Zachara J. M. (1992). Chemical Contaminants on DOE Lands and Selection of Contaminant Mixtures for Subsurface Science Research. *DOE/ER-0547T*, US Department of Energy, Washington, DC.

River Protection Project, R.P.P. (2005). Field Investigation Report for Waste Management Area T-TX-TY. *RPP-23752*, CH2M Hill Hanford Group, Richland, WA.

Rucker D. F. and Fink J. B. (2007) Inorganic plume delineation using surface high resolution electrical resistivity at the BC cribs and trenches site, Hanford. *Vadose Zone J.* **64**, 946–958.

Serne, R. J. and Mann, F. M. (2004). Preliminary Data from 216-B-26 Borehole in BC Cribs Area. *RPP-20303, Rev. 0*, CH2M Hill Group, Richland, WA.

Stone A. T. and Morgan J. J. (1984) Reduction and dissolution of manganese(III) and manganese(IV) oxides by organics 2. Survey of the reactivity of organics. *Environ. Sci. Technol.* **18**, 617–624.

Tischendorf G., Forster H.-J., Gottesmann B. and Rieder M. (2007) True and brittle micas: composition and solid-solution series. *Mineral. Mag.* **71**, 285–320.

Weaver C. E. and Pollard L. D. (1975) The Chemistry of Clay Minerals. Elsevier Science Publishing Company, New York, NY.

Wildung R. E., Gorby Y. A., Krupka K. M., Hess N. J., Li S. W., Plymale A. E., McKinley J. P. and Fredrickson J. K. (2000) Effect of electron donor and solution chemistry on products of dissimilatory reduction of technetium by *Shewanella putrefaciens*. *Appl. Environ. Microbiol.* **66**, 2451–2460.

Wildung R. E., Li S. W., Murray C. J., Krupka K. M., Xie Y., Hess N. J. and Roden E. E. (2004) Technetium reduction in sediments of a shallow aquifer exhibiting dissimilatory iron reduction potential. *FEMS Microbiol. Ecol.* **49**, 151–162.

Zachara J. M., Gassman P. L., Smith S. C. and Taylor D. (1995) Oxidation and adsorption of Co(II) $EDTA^{2-}$ complexes in a subsurface materials with iron and manganese oxides. *Geochim. Cosmochim. Acta* **59**, 4449–4463.

Zachara J. M., Fredrickson J. K., Li S. W., Kennedy D. W., Smith S. C. and Gassman P. L. (1998) Bacterial reduction of crystalline Fe^{3+} oxides in single phase suspensions and subsurface materials. *Am. Mineral.* **83**, 1426–1443.

Zachara J. M., Fredrickson J. K., Kukkadapu R. K. and Gorby Y. A. (2007a). *Anaerobic microbial-mineral processes with Fe(III) oxides: experimental considerations and approaches.* Methods for Investigating Microbial–Mineral Interactions.

Zachara J. M., Heald S. M., Jeon B. H., Kukkadapu R. K., Liu C. X., McKinley J. P., Dohnalkova A. C. and Moore D. A. (2007b) Reduction of pertechnetate [Tc(VII)] by aqueous Fe(II) and the nature of solid phase redox products. *Geochim. Cosmochim. Acta* **71**, 2137–2157.

Zachara J. M., Serne R. J., Freshley M. D., Mann F., Anderson F., Wood M., Jones T. and Myers D. (2007c) Geochemical processes controlling migration of high level wastes in Hanford's vadose zone. *Vadose Zone J.* **64**, 985–1003.

Associate editor: Eric H. Oelkers